Journal of the European Ceramic Society xxx (xxxx) xxx–xxx

Contents lists available at ScienceDirect

Journal of the European Ceramic Society

journal homepage: www.elsevier.com/locate/jeurceramsoc

Original Article

Bismuth borate composite microwave ceramics synthesised by different ratios of H_3BO_3 for ULTCC technology

Kangguo Wang, Tingting Yin, Huanfu Zhou*, Xiaobin Liu, Jiji Deng, Shixuan Li, Chengming Lu, Xiuli Chen

Collaborative Innovation Center for Exploration of Hidden Nonferrous Metal Deposits and Development of New Materials in Guangxi, Key Laboratory of Nonferrous Materials and New Processing Technology, Ministry of Education, School of Materials Science and Engineering, Guilin University of Technology, Guilin 541004, China

ARTICLE INFO

Keywords:
Bismuth borate composite
Ultra-low-temperature cofired ceramic
Microwave dielectric properties

ABSTRACT

$Bi_3B_{5+x}O_{12+3x/2}$ ($x = 0 \sim 6$) compounds were fabricated by a conventional solid-state reaction method. The microwave dielectric properties, sintering behaviour, crystal structure, and phase evolution of the ceramics were investigated. All samples densified at ultra-low temperatures (575 ~ 700 °C). As x increased, the phase composition of the ceramics gradually changed from mixed $Bi_4B_2O_9$ and $Bi_3B_5O_{12}$ phases to a single $Bi_6B_{10}O_{24}$ phase. The ceramic with $x = 4$ exhibited the best microwave dielectric properties of $\varepsilon_r = 12.14$, $Q \times f = 14{,}800$ GHz, and $\tau_f = -72$ ppm/°C at 625 °C. The microwave dielectric properties deteriorated as x increased further. Moreover, the ceramics were proven to cofire with Al and Ag, indicating that they are candidates for ultra-low-temperature cofired ceramic devices.

1. Introduction

With the accelerating development of the modern wireless communication industry and wearable electronic devices, low-temperature cofired ceramic (LTCC) technology is receiving attention because it can improve the portability of the equipment [1,2]. Ceramics with good microwave dielectric properties and low sintering temperatures (≤900 °C) are demanded by LTCC technology [3,4]. With the rapid development of flexible wearable electronics, ceramics also need to cofire with various low melting point (below 700 °C) materials, such as Al electrode materials, semiconductor materials, polymer substrates, etc [5–9].

Recently, many ceramics with excellent microwave dielectric properties and ultra-low sintering temperatures (below 700 °C), such as $CuMoO_4$ [10,11], $10Li_2O$–$10Na_2O$–$20K_2O$–$60MoO_3$ [12], Bi_2O_3–TeO_2 [13], and α-MoO_3, have been researched [14]. However, research on ultra-LTCC (ULTCC) is still very limited and insufficient. Low sintering temperatures mean low cost, so research into ULTCC systems is urgently required.

$Bi_6B_{10}O_{24}$ ceramic exhibits good microwave dielectric properties ($\varepsilon_r = 10$, $Q \times f = 10{,}800$ GHz, and $\tau_f = -41$ ppm/°C) and a low sintering temperature (700 °C) [15]. However, its sintering temperature is too high for it to be cofired with Al electrodes (melting at 660 °C). As a cosolvent material, H_3BO_3 has a lower melting point (171 °C) and weaker BO− covalent bonds than B_2O_3 (450 °C) [16]. Hence, synthesis of $Bi_6B_{10}O_{24}$ using H_3BO_3 may reduce the sintering temperature. In this work, $Bi_3B_{5+x}O_{12+3x/2}$ ($x = 0 \sim 6$) composite ceramics were designed and prepared using H_3BO_3 and Bi_2O_3 powders. Furthermore, the ceramics' sintering behaviours, microstructures, microwave dielectric properties, and compatibilities with aluminium and silver were investigated.

2. Experimental procedure

$Bi_3B_{5+x}O_{12+3x/2}$ ($x = 0 \sim 6$) ceramics were prepared by a conventional solid-state reaction method. High-purity raw powders of Bi_2O_3 (99.95%) and H_3BO_3 (99.99%) were stoichiometrically weighted, mixed, and ball milled in alcohol with zirconia balls for 6 h and then dried at 90 °C in a drying oven. Subsequently, the dry powders were calcined in air at 575 °C for 4 h. The fine calcined powders were granulated by using 5 wt% polyvinyl alcohol (PVA) and then pressed into cylinders with a diameter of 10 mm and thickness of 4–6 mm under a pressure of approximately 200 MPa. Finally, the disks were heated in air to 550 °C for 4 h to exhaust the binder and then sintered at 550–700 °C for 4 h at a heating rate of 5 °C/min.

The crystalline phases of the ceramics were determined by an X-ray diffractometer (XRD; Model X'Pert PRO, PANalytical, Almelo, Netherlands) with a scan rate of 0.417°/s and Cu Kα radiation

* Corresponding author.
E-mail address: zhouhuanfu@163.com (H. Zhou).

https://doi.org/10.1016/j.jeurceramsoc.2019.09.035
Received 10 May 2019; Received in revised form 16 September 2019; Accepted 20 September 2019

generated at 40 kV and 40 mA. To calculate the relative phase contents further, Rietveld refinement data were obtained at a low scan rate (0.021°/s) using GSAS software. Scanning electron microscopy (SEM; Model JSM6380-LV, JEOL, Tokyo, Japan) was used to observe the microstructures of the natural surfaces of the ceramics. In thermal etching, all cross sections of samples were polished and heated at 50 °C below their sintering temperature for 30 min. The relative densities of the ceramics were calculated using Eq. (1):

$$\rho_r = \rho_b/\rho_C, \tag{1}$$

where ρ_r, ρ_b, and ρ_C are the relative density, bulk density, and theoretical density of the ceramics, respectively. The bulk density was measured by Archimedes method. The theoretical density was calculated using Eq. (2):

$$\rho_C = \frac{1}{(^{M1}/_{\rho_1}) + (^{M2}/_{\rho_2})}, \tag{2}$$

where M1, M2 and ρ_1, ρ_2 are the mass fraction and the theoretical density of a single distinct component, respectively. The mass fraction ratio of the $Bi_4B_2O_9$ and $Bi_6B_{10}O_{24}$ phases was calculated by the reference intensity ratio (RIR) method. [17]

The dielectric behaviour in the microwave frequency range was tested by the TE01δ method using a network analyser (E5071C, Agilent Co., CA, USA, 10 MHz to 20 GHz). The temperature coefficients of resonant frequency (τ_f) values were calculated using Eq. (3):

$$\tau_f = \frac{f_T - f_0}{f_{T_0}(T - T_0)} \tag{3}$$

where f_T and f_{T_0} are the resonant frequencies at 80 °C and 25 °C, respectively.

3. Results and discussion

Fig. 1 shows the bulk density and relative density of the $Bi_3B_{5+x}O_{12+3x/2}$ ($x = 0 \sim 6$) ceramics at the optimum sintering temperature. The bulk density of $Bi_3B_{5+x}O_{12+3x/2}$ ceramics as a function of sintering temperature is shown in FIG. S1 (Supplementary Data). The relative densities of all samples were above 90%. As x continued to increase, the bulk density value for the ceramics decreased from 6.75 g/cm^3 to 5.89 g/cm^3 and then became stable at approximately 5.8 g/cm^3. However, when $x < 4$, there was an opposite trend between relative density and bulk density as x increased. Phase transition caused a decrease in the theoretical density, which led to a completely opposite relationship between bulk density and relative density according to Eq. (1) in Section 2. The relative density reached a maximum of 95.25% and then remained stable.

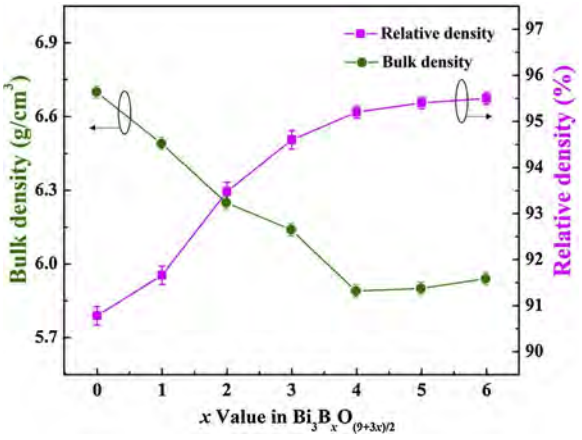

Fig. 1. Bulk density and relative density of the $Bi_3B_{5+x}O_{12+3x/2}$ ceramics ($x = 0 \sim 6$) at the optimum sintering temperature.

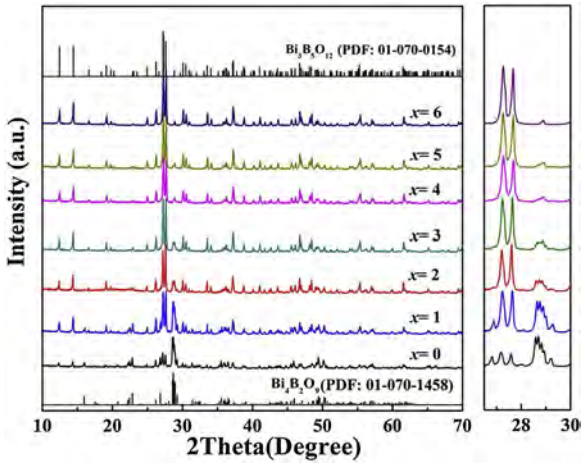

Fig. 2. XRD patterns of the $Bi_3B_{5+x}O_{12+3x/2}$ ceramics at room temperature after sintering at the optimum temperature.

Fig. 2 shows the XRD patterns of the $Bi_3B_{5+x}O_{12+3x/2}$ ceramics at room temperature, after they were sintered at the optimum sintering temperature. When $x = 0$, the main peak of the ceramic appeared at $2\theta = 28.6$, which matches well with the $Bi_4B_2O_9$ phase. This result can be explained by the volatilisation of H_3BO_3 with moisture in the air. With increase of the H_3BO_3 ratio, the monoclinic $Bi_4B_2O_9$ phase transformed into an orthorhombic $Bi_6B_{10}O_{24}$ phase. As x increased to ≥ 4, all peaks of the ceramics were indexed as orthorhombic $Bi_6B_{10}O_{24}$ (PDF: 01-070-0154), indicating that a single phase had been obtained.

To demonstrate the phase proportions further, the theoretical densities and mass ratios of the $Bi_4B_2O_9$ and $Bi_6B_{10}O_{24}$ phases are listed in Table S1. The mass fraction ratio of $Bi_6B_{10}O_{24}$ increased from 28.74% to 80.09% as x increased from 0 to 3. It is known that the calculated bulk density of $Bi_4B_2O_9$ of 8.18 g/cm^3 is higher than the calculated bulk density of $Bi_6B_{10}O_{24}$ of 6.20 g/cm^3 [15]. Hence, the theoretical density of the $Bi_3B_{5+x}O_{12+3x/2}$ ceramics attains a lower value at high ranges of x. This result could explain why the relative density increased as x increased, even though the bulk density decreased.

Fig. 3 shows the result of the Rietveld refinement analysis for the $Bi_3B_{5+x}O_{12+3x/2}$ ($x = 4$) sample. The refined cell parameters were a = 6.5390(6) Å, b = 7.7405(7) Å, c = 18.5763(15) Å, V = 940.24(10) Å^3, and $\alpha = \beta = \gamma = 90°$. The small R-values (Rp = 7.51%, Rwp = 9.73%, Rexp = 3.07%) indicated that the measurements of the XRD patterns for the ceramic matched extremely well with the theoretical model of $Bi_6B_{10}O_{24}$ (PDF: 01-070-0154) with orthorhombic structure in space group Pnma(62). The atomic coordinates are

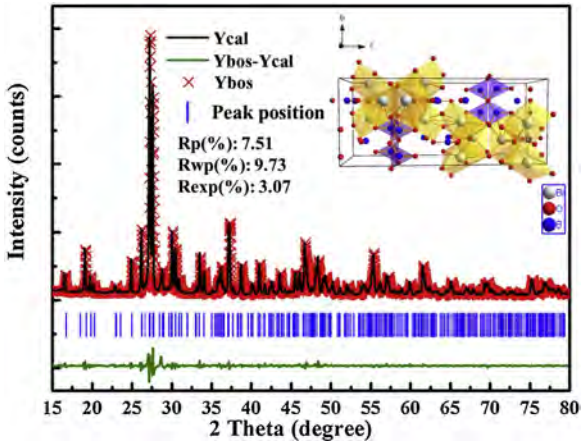

Fig. 3. Rietveld refinement of the room-temperature XRD data. The inset shows a crystal structure schematic of the $Bi_3B_{5+x}O_{12+3x/2}$ ($x = 4$) ceramic.

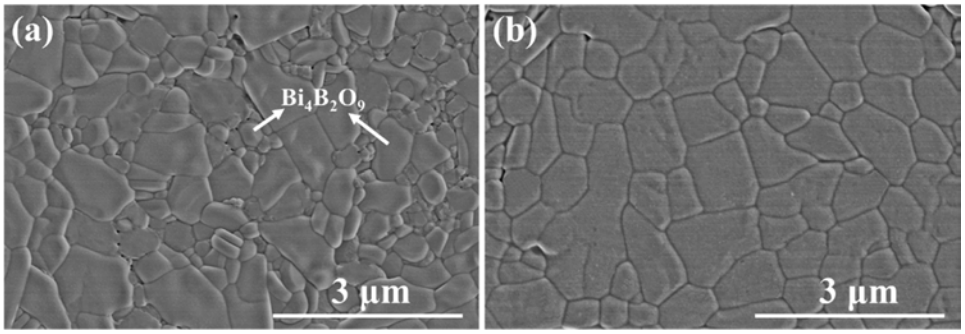

Fig. 4. SEM images of the polished and thermally etched cross sections of the $Bi_3B_{5+x}O_{12+3x/2}$ ceramics. (a) $x = 0$ at 575 °C; (b) $x = 4$ at 625 °C.

summarised in Table S2. The inset of Fig. 3 shows the B and O atom connections forming a tetrahedron in the ceramic and the Bi atom existing in the form of a polyhedron formed by connecting one B atom and several O atoms. This result agrees well with the $Bi_3B_5O_{12}$ crystal structure analysis in Filatov's work [18].

Fig. 4 shows SEM images of the polished and thermally etched cross sections of the $Bi_3B_{5+x}O_{12+3x/2}$ ceramics ($x = 0$, $x = 4$) after sintering at the optimum temperatures. The EDS analysis of Fig. 4 is listed in Table S3. All samples exhibited a compact structure due to densification at the optimum sintering temperature. However, Fig. 4(a) shows the different grain sizes and the second phase, $Bi_4B_2O_9$, in the ceramic. Combining this result with the XRD analysis results, it is apparent that the two phases in coexistence led to the different grain sizes in the ceramics. As x increased, because of the disappearance of the second phase, the grain size of the ceramic became unified, and the structure became more compact. When $x = 4$, clear and unified grain sizes were observed, as shown in Fig. 4(b).

Fig. 5 shows the variations of the sintering temperature, ε_r, $Q \times f$, and τ_f values of the $Bi_3B_{5+x}O_{12+3x/2}$ ceramics as a function of x. All samples could be densified below 650 °C. Pure $Bi_6B_{10}O_{24}$, which densified at 700 °C, was fabricated by Chen et al. [15]. Lower sintering temperature makes it possible to cofire the ceramics with Al. The ε_r value is affected by the phase composition, ionic polarisability, and degree of densification [16,17]. Because the ceramics sintered at optimum temperature could achieve high densification, the phase composition would determine the variation of the relative permittivity. As x increased, ε_r first decreased significantly, then reached the small value of 10.94 at $x = 4$, and finally remained a stable constant. The ε_r values of $Bi_4B_2O_9$ and $Bi_6B_{10}O_{24}$ in Chen's work were 39 and 10, respectively [15]. The downward trend of the relative permittivity can be explained well by the phase evolution of $Bi_4B_2O_9$ translated into $Bi_6B_{10}O_{24}$.

There are two types of losses that influence microwave dielectric loss: intrinsic and extrinsic losses. Usually, intrinsic losses are determined by crystal lattice vibrations, and extrinsic losses are determined by multiple factors, such as the secondary phases, morphology, and pore size of the materials [18–20]. As depicted in the XRD results, a notable phase transition appeared in the $Bi_3B_{5+x}O_{12+3x/2}$ ceramics as x increased. The phase transition of $Bi_4B_2O_9$ into $Bi_6B_{10}O_{24}$ significantly improved the $Q \times f$ of the $Bi_3B_{5+x}O_{12+3x/2}$ ceramics. When $x = 4$, the ceramic exhibited a high $Q \times f$ value of 14,750 GHz due to the single $Bi_6B_{10}O_{24}$ phase. With further increase of x values, the $Q \times f$ decreased to 9,530 GHz, which could have been caused by the increase of B_2O_3 aggregates at grain boundaries.

The τ_f is closely related to the permittivity and structural phase transitions of a material, and it is affected by secondary phases and the preferred orientation of grains [21–23]. The phase evolution was the main factor influencing the τ_f of the ceramics. Chen [15] reported that the τ_f value of $Bi_4B_2O_9$ is much lower than the value of $Bi_6B_{10}O_{24}$ ($Bi_4B_2O_9 = -203$; $Bi_6B_{10}O_{24} = -41$). However, in our work, τ_f shows a downward trend from –55 to –73 ppm/°C with increase of x values. τ_f values can be calculated using the mixing rule shown in Eq. 4:

$$\tau f = \sum_{i}^{n} v_i \tau_{fi} \tag{4}$$

where v_i and τ_{fi} are the volume fraction and temperature coefficient of the resonant frequency of the ith phase, respectively. Because the volume fraction of $Bi_4B_2O_9$ decreases with increase of x value, the downward trend of τ_f suggests that the τ_f value of $Bi_4B_2O_9$ is higher than that of $Bi_6B_{10}O_{24}$. This result is quite different from the literature. If the x value is reduced to -2, the single phase of $Bi_4B_2O_9$ will show a temperature coefficient of -52 ppm/°C (microwave dielectric properties are shown in Table 1).

The chemical compatibility between the $Bi_3B_{5+x}O_{12+3x/2}$ ($x = 4$) ceramic and Al was tested. The Al phase was identified from the XRD

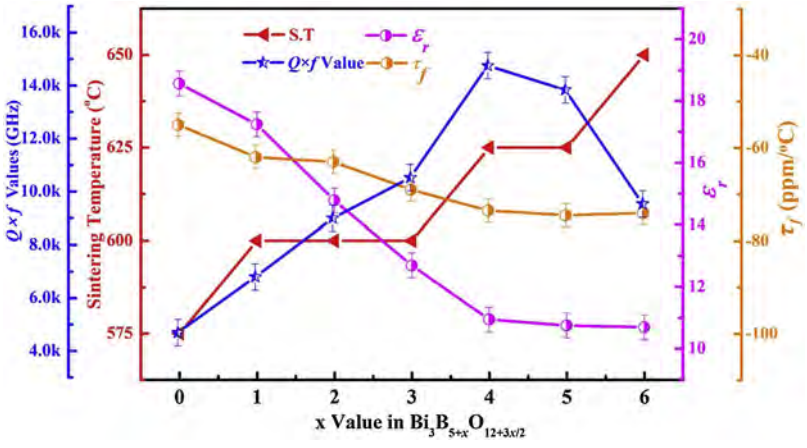

Fig. 5. Sintering temperature, microwave dielectric constant, $Q \times f$ values, and τ_f values of the $Bi_3B_{5+x}O_{12+3x/2}$ ceramics as a function of x values.

Table 1
Comparison of the microwave dielectric properties of some compounds with low relative permittivity and sintering temperature.

Composition	*Ts* (°C)	$Q \times f$ (GHz)	ε_r	τ_f (ppm/°C)	Reaction with Al	*Ref*
$Bi_6B_{10}O_{24}$	700	10,800	10	−41	–	[15]
$Nd_4Mo_4O_{15}$	700	61,500	11.1	−44	–	[24]
$Li_3FeMo_3O_{12}$	580	12,000	11.5	−20	–	[25]
BaV_2O_6	550	42,790	11.2	28.2	No	[26]
$Bi_3B_{5+x}O_{12+3x/2}$ ($x = -2$)	575	3,300	39	−52	–	This work
$Bi_3B_{5+x}O_{12+3x/2}$ ($x = 4$)	625	14,800	12.1	−72	No	This work
$Mg_3V_2O_8$	750	11,000	4.5	−60	–	[27]

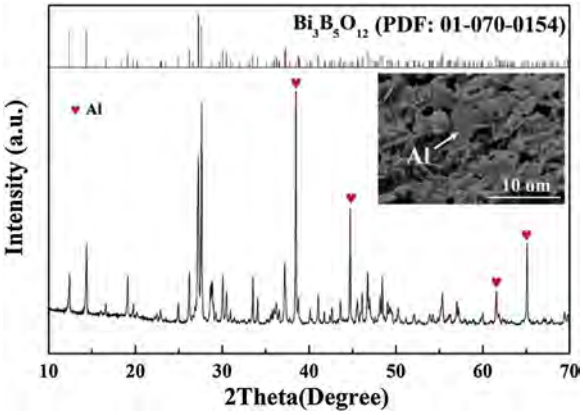

Fig. 6. XRD patterns and SEM image of $Bi_3B_{5+x}O_{12+3x/2}$ ($x = 4$) ceramic with 50% Al powder.

patterns and SEM image in Fig. 6, and the results indicated that the phase composition of $Bi_3B_{5+x}O_{12+3x/2}$ ($x = 4$) ceramic did not change with the addition of Al. Additionally, the $Bi_3B_{5+x}O_{12+3x/2}$ ($x = 4$) ceramic had no reaction with Ag at 625 °C, as shown in FIG. S2. These results suggest that $Bi_3B_{5+x}O_{12+3x/2}$ ($x = 4$) ceramic is a good candidate for ULTCC materials.

Some microwave dielectric ceramics with low relative permittivity and sintering temperature are summarised in Table 1. Molybdates, such as $Nd_4Mo_4O_{15}$ [24], $Li_3FeMo_3O_{12}$ [25] vanadates, such as BaV_2O_6 [26], and $Mg_3V_2O_8$ [27] exhibit good microwave dielectric properties; however, high raw cost restricts their further applications. $Bi_6B_{10}O_{24}$ has good microwave dielectric properties, but its high sintering temperature of ~700 °C hinders its co-firing with Al electrode. By contrast, $Bi_6B_{10}O_{24}$ ceramic with excessive ratio H_3BO_3 exhibits good microwave dielectric properties and also has good compatibility with Al electrode, showing that it is a good candidate for ULTCC devices.

4. Conclusion

$Bi_3B_{5+x}O_{12+3x/2}$ ($x = 0 \sim 6$) ULTCCs with low relative permittivity and high $Q \times f$ were investigated. As x increased from 0 to 6, the phase composition converted from two phases to a single phase, and the microwave dielectric properties of the $Bi_3B_{5+x}O_{12+3x/2}$ ceramics changed significantly. When $x = 4$, the $Bi_3B_{5+x}O_{12+3x/2}$ ceramic exhibited a single $Bi_6B_{10}O_{24}$ phase and the best microwave dielectric properties of $\varepsilon_r = 12.14$, $Q \times f = 14{,}800$ GHz, and $\tau_f = -72$ ppm/°C. The $Bi_3B_{5+x}O_{12+3x/2}$ ($x = 0 \sim 6$) ceramics could also be cofired with Al and Ag, demonstrating the potential of $Bi_3B_{5+x}O_{12+3x/2}$ ceramic for wide utilisation in a new class of ULTCCs or LTCCs for multilayer applications.

Acknowledgments

This work was supported by the Natural Science Foundation of China (Nos. 61761015 and 11664008), and the Natural Science Foundation of Guangxi (Nos. 2017GXNSFFA198011 and 2017GXNSFDA198027).

Appendix A. Supplementary data

Supplementary material related to this article can be found, in the online version, at doi:https://doi.org/10.1016/j.jeurceramsoc.2019.09.035.

References

[1] L.X. Pang, D. Zhou, Z.M. Qi, W.G. Liu, Z.X. Yuee, I.M. Reaney, Structure-property relationships of low sintering temperature scheelite-structured (1 − x) $BiVO_4$–x$LaNbO_4$ microwave dielectric ceramics, J. Mater. Chem. C 5 (2017) 2695–2701.
[2] K.G. Wang, H.F. Zhou, X.B. Liu, W.D. Sun, X.L. Chen, H. Ruan, A lithium aluminium borate composite microwave dielectric ceramic with low permittivity, near-zero shrinkage, and low sintering temperature, J. Eur. Ceram. Soc. 39 (4) (2019) 1122–1126.
[3] M.T. Sebastian, H. Jantunen, Low loss dielectric materials for LTCC applications: a review, J. Int. Mater. Rev. 53 (2) (2008) 57–90.
[4] H.F. Zhou, K.G. Wang, W.D. Sun, X.L. Chen, H. Ruan, Phase composition, singtering behavior and microwave dielectric properties of $M_2BiLi_2V_3O_{12}$ (M = Zn, Ca) low temperature co-fired ceramics, Mater. Lett. 217 (15) (2018) 20–22.
[5] M.T. Sebastian, H. Wang, H. Jantunen, Low temperature co-fired ceramics with ultra-low sintering temperature: a review, J. Curr. Opin. Solid. State Mater. 20 (3) (2016) 151–170.
[6] J. Varghese, T. Siponkoski, M. Sobocinski, T. Vahera, H. Jantunen, Multilayer functional Tapes Cofired at 450 °C: beyond HTCC and LTCC technologies, ACS Appl. Mater. Interfaces 10 (13) (2018) 11048–11055.
[7] J. Varghese, P. Ramachandran, M. Sobocinski, T. Vahera, H. Jantunen, ULTCC glass composites based on rutile and Anatase with cofiring at 400 °C for high frequency applications, ACS Sustain. Chem. Eng. 7 (4) (2019) 4274–4283.
[8] D. Zhou, C.A. Randall, H. Wang, et al., Microwave dielectric ceramics in Li_2O–Bi_2O_3–MoO_3 system with ultra–low sintering temperatures, J. Am. Ceram. Soc. 93 (4) (2010) 1096–1100.
[9] M. Udovic, M. Valant, D. Suvorov, Phase formation and dielectric characterization of the Bi_2O_3–TeO_2 System prepared in an oxygen atmosphere, J. Am. Ceram. Soc. 87 (4) (2004) 91–97.
[10] N. Joseph, J. Varghese, T. Siponkoski, M. Teirikangas, M.T. Sebastian, H. Jantunen, Glass-free $CuMoO_4$ Ceramic with excellent dielectric and thermal properties for ultralow temperature cofired ceramic applications, ACS Sustain. Chem. Eng. 4 (10) (2016) 5632–5639.
[11] N. Joseph, J. Varghese, M. Teirikangas, M.T. Sebastian, H. Jantunen, Ultra-low sintering temperature ceramic composites of $CuMoO_4$ through Ag_2O addition for microwave applications, Compos. Part B-Eng. 141 (15) (2018) 214–220.
[12] J. Varghese, T. Siponkoski, M. Teirikangas, M.T. Sebastian, A. Uusimaki, H. Jantunen, Dielectric, and thermal properties of Pb free molybdate based ultralow temperature glass, ACS Sustain. Chem. Eng. 4 (7) (2016) 3897–3904.
[13] M. Udovic, M. Valant, D. Suvorov, Phase formation and dielectric characterization of the Bi_2O_3–TeO_2 System prepared in an oxygen atmosphere, J. Am. Ceram. Soc. 87 (4) (2004) 91–97.
[14] J. Varghese, T. Siponkoski, M. Nelo, M.T. Sebastian, H. Jantunen, Microwave dielectric properties of low-temperature sinterable α-MoO_3, J. Eur. Ceram. Soc. 38 (4) (2018) 1541–1547.
[15] X.Y. Chen, W.J. Zhang, B. Zalinska, I. Sterianou, S.X. Bai, I.M. Reaney, Low sintering temperature microwave dielectric ceramics and composites based on Bi_2O_3 –B_2O_3, J. Am. Ceram. Soc. 95 (10) (2012) 3207–3213.
[16] J.D. Joyner, M.D. Hercules, Chemical bonding and electronic structure of B_2O_3, H_3BO_3, and BN: An ESCA, Auger, SIMS, and SXS study, J. Chem. Phys. 72 (2) (1980) 1095–1108.
[17] S.S.A. Jaroudi, A.U. Hamid, A.R.I. Mohammed, S. Saner, Use of X-ray powder diffraction for quantitative analysis of carbonate rock reservoir samples, Powder Technol. 175 (3) (2007) 115–121.
[18] S. Filatov, Y. Shepelev, R. Bubnova, N. Sennova, A.V. Egorysheva, Y.F. Karginc, The study of $Bi3B_5O_{12}$: synthesis, crystal structure and thermal expansion of oxoborate $Bi_3B_5O_{12}$, J. Solid State Chem. 177 (3) (2004) 515–522.
[19] S. George, M.T. Sebastian, Synthesis and microwave dielectric properties of novel temperature stable high q, $Li_2ATi_3O_8$ (A = Mg, Zn) ceramics, J. Eur. Ceram. Soc.

(30) (2010) 2585–2592.
[20] H.C. Xiang, C.C. Li, H.L. Jantunen, L. Fang, A.E. Hill, Ultralow loss $CaMgGeO_4$ microwave dielectric ceramic and its chemical compatibility with silver electrodes for low-temperature cofired ceramic applications, ACS Sustain. Chem. Eng. (6) (2018) 6458–6466.
[21] W. Lei, Z.Y. Zou, Z.H. Chen, B. Ullah, A. Zeb, X.K. Lan, We.Z. Lu, G.F. Fan, X.H. Wang, X.C. Wang, Controllable τ_f value of barium silicate microwave dielectric ceramics with different Ba/Si ratios, J. Am. Ceram. Soc. 101 (25) (2018) 25–30.
[22] X.G. Wu, H. Wang, Y.H. Chen, D. Zhou, Synthesis and microwave dielectric properties of $Zn_3B_2O_6$ ceramics for substrate application, J. Am. Ceram. Soc. 95 (6) (2012) 1793–1795.
[23] S.J. Penn, N.M. Alford, A. Templeton, X. Wang, M. Xu, M. Reece, K. Schrapel, Effect of porosity and grain size on the microwave dielectric properties of sintered alumina, J. Am. Ceram. Soc. 80 (7) (1997) 1885–1888.
[24] A. Surjith, E.K. Suresh, R. Ratheesh, Microwave dielectric properties of low temperature sinterable $RE_2MO_4O_{15}$ (Re = Nd, Sm) ceramics for LTCC applications, J. Mater. Sci. Mater. Electr. 24 (2013) 1818–1822.
[25] Q. Liao, Y.L. Wang, F. Jiang, D. Guo, Ultra-low fire glass-free $Li_3FeMo_3O_{12}$ microwave dielectric ceramics, J. Am. Ceram. Soc. 97 (8) (2014) 2394–2396.
[26] U.A. Neelakantan, S.E. Kalathil, R. Ratheesh, Structure and microwave dielectric properties of ultralow-temperature cofirable BaV_2O_6 ceramics, Eur. J. Inorg. Chem. 2 (2015) 305–310.
[27] R. Umemura, H. Ogawa, A. Kan, Low temperature sintering and microwave dielectric properties of $(Mg_{3-x}Zn_x)(VO_4)_2$ ceramics, J. Eur. Ceram. Soc. 26 (2006) 2063–2068.